Phase transitions and spin-state of iron in FeO at the conditions of Earth's deep interior

E. Greenberg,[1,*] R. Nazarov,[2,*] A. Landa,[2] J. Ying,[3,4] R. Q. Hood,[2] B. Hen,[5] R. Jeanloz,[6] V. B. Prakapenka,[1] V. V. Struzhkin,[7] G. Kh. Rozenberg,[5] and I. V. Leonov[8,9,10]

[1]*Center for Advanced Radiation Sources, University of Chicago, 5640 South Ellis Avenue, Chicago, Illinois 60637, USA*
[2]*Physics Division, Physical and Life Sciences Directorate, Lawrence Livermore National Laboratory, Livermore, CA 94551*
[3]*Geophysical Laboratory, Carnegie Institution of Washington, Washington, DC 20015, USA*
[4]*Department of Physics, University of Science and Technology of China, Hefei, Anhui 230026, China*
[5]*Raymond and Beverly Sackler School of Physics and Astronomy, Tel-Aviv University, Tel Aviv 69978, Israel*
[6]*Departments of Earth and Planetary Science and Astronomy, and Miller Institute for Basic Research in Science, University of California, Berkeley, California 94720, USA*
[7]*Center for High Pressure Science and Technology Advanced Research, Shanghai, China*
[8]*M.N. Miheev Institute of Metal Physics, Russian Academy of Sciences, 620108 Yekaterinburg, Russia*
[9]*Ural Federal University, 620002 Yekaterinburg, Russia*
[10]*Skolkovo Institute of Science and Technology, 143026 Moscow, Russia*

Iron-bearing oxides undergo a series of pressure-induced electronic, spin and structural transitions that can cause seismic anomalies and dynamic instabilities in Earth's mantle and outer core. We employ x-ray diffraction and x-ray emission spectroscopy along with DFT+dynamical mean-field theory calculations to characterize the electronic structure and spin states, and crystal-structural properties of wüstite ($Fe_{1-x}O$) – a basic oxide component of Earth's interior – at high pressure-temperature conditions up to 140 GPa and 2100 K. We find that FeO exhibits complex polymorphism under pressure, with abnormal compression behavior associated with electron-spin and crystallographic phase transitions, and resulting in a substantial change of bulk modulus. Our results reveal the existence of a high-pressure phase characterized by a metallic high-spin state of iron near to the pressure-temperature conditions of Earth's core-mantle boundary. The presence of high-spin metallic iron near the base of the mantle can significantly influence the geophysical and geochemical properties of Earth's deep interior.

Iron monoxide, wüstite ($Fe_{1-x}O$), is among the most representative of compounds making up the terrestrial planets: as an electrically insulating oxide, it is akin to the constituents of rocky mantles, yet it can also be a metallic alloy, such as comprises planetary cores [1–3]. Because it is likely a major component of Earth's core, and may also be present near the mantle-core boundary due to interactions between Earth's rocky and liquid-metal regions, characterization of wüstite at high pressures and temperatures is fundamental to understanding the nature and evolution of our and other planets deep interior [4–10]. Notably, this one oxide exhibits a richness of condensed-matter phenomena that can significantly influence mantle convection, plume stability and other aspects of planetary internal dynamics, including crystal-structural phase transformations and melting, electronic (e.g., insulator-to-metal) transitions, and spin-state transitions that affect atomic structure and magnetic moments [11, 12]. An end-member of magnesiowüstite [(Mg, Fe)O], the second most abundant mineral of Earth's mantle, wüstite exhibits (under pressure) spin-state transitions and other key features of our planet's most abundant but more complex mineral compound, $(Mg,Fe)SiO_3$ bridgmanite [11].

Wüstite has a rich phase diagram featuring at least five crystallographic phases, from the rock-salt B1 (NaCl) (or low-temperature rhombohedral rB1) to cubic B2 (CsCl) structure [4–9, 13–16]. A Mott insulator with a relatively large band gap of ∼2.4 eV at ambient conditions, it is known to undergo a Mott insulator-to-metal phase transition (IMT) under pressure [5, 13–19]. This metallization transition has been claimed to be accompanied by a high-spin (HS) to low-spin (LS) electronic transition in iron. Contraction of the iron ionic volume by up to ∼20-40 percent at the spin transition results in dramatic changes in seismological (density, elasticity) and transport properties (e.g., electrical and thermal conductivity), as well as in chemical partitioning of iron-bearing minerals [11, 12, 20, 21]. Therefore, documenting the electronic state of iron in FeO (and other iron-bearing minerals [23–32]) is thought to be essential for understanding the structure and evolution of Earth's lower mantle and core-mantle boundary. However, despite being an archetype for terrestrial planetary materials, FeO is poorly understood, and its phase diagram and electronic properties remain controversial, especially at high pressure and temperatures [4–9, 11–22, 33–35].

In our present study, we address these gaps in understanding and examine the phase diagram of FeO

*These authors contributed equally to this work.

[13, 14] using state-of-the-art quantum mechanical DFT+dynamical mean-field theory (DFT+DMFT) calculations [38–41], along with x-ray diffraction (XRD) and x-ray emission spectroscopy (XES) measurements at simultaneously high temperatures and pressures [42] to determine the crystal structures, electronic and spin state of FeO over a wide range of pressures. Using DFT+DMFT it becomes possible to determine on the same footing the details of a pressure-driven Mott IMT, change in crystal structure and collapse of local moments of FeO. Our results document the interplay between electron correlation and delocalization (i.e., metallic character) that – along with changes in crystal structure and iron spin-state – makes for rich allotropic behavior and significant variations in elastic properties.

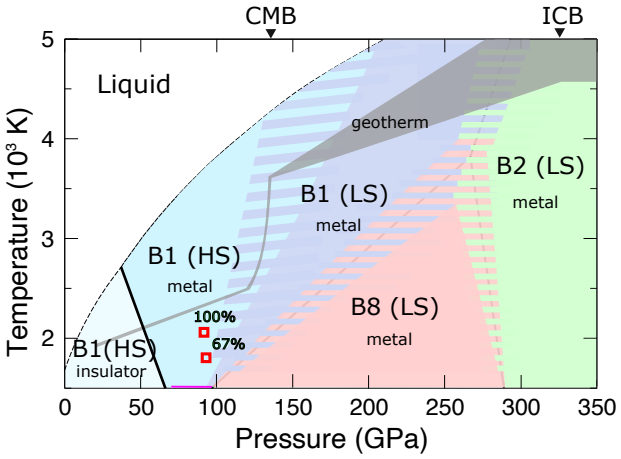

FIG. 1: Pressure-temperature phase diagram of PM FeO evaluated from the DFT+DMFT crystal-structural calculations. Our results for the phase equilibria among the rock-salt B1 (NaCl), normal and inverse B8 (NiAs and anti-NiAs), and cubic B2 (CsCl) crystal phases are shown, as is the distinction between the HS and LS Fe. The melting curve (dashed black lines) is from previous experiments (see Ref. 22 and references therein), and the pressures at the core-mantle boundary (CMB) and inner-core boundary (ICB) are indicated at the top, along with inferred temperatures inside Earth (geotherm: gray). Our XRD and XES data at pressures near 90 GPa show only the presence of the HS B1 phase at ∼2000 K and about 67% HS Fe in a mixture of the rB1 and B1 structures at ∼1800 K (red squares). We note that the calculated B1-B8 and B8-B2 phase boundaries are in agreement with the experimental data [6, 9, 13, 36, 37].

We start by computing the pressure-temperature phase diagram of paramagnetic (PM) FeO at temperatures above 1200 K using DFT+DMFT, taking into account the B1 (NaCl-type), B2 (CsCl-type), B8 (NiAs-type) and inverse B8 (Fe and O sites interchanged from B8) crystal structures (Figs. 1, 2). We employ a fully self-consistent in charge density DFT+DMFT method [17–19] implemented with plane-wave pseudopotentials in DFT [43, 44] and continuous-time hybridization-expansion quantum Monte-Carlo algorithm in DMFT [45]. In the DFT+DMFT calculations for the Fe $3d$ and O $2p$ valence states we construct a basis set of atomic-centered Wannier functions within the energy window spanned by these bands [46–48]. The effects of electron correlations in the Fe $3d$ shell are described using a Coulomb interaction U ranging from 7 to 9 eV, as estimated for the different crystallographic phases (near thier stabilty range) within constrained DFT [48, 49]; also, we take the Hund's exchange energy $J = 0.86$ eV. In our calculations we neglect the possible pressure-dependence of the Hubbard U and Hund's J values [35, 50], whose variation upon compression is assumed to be small. Further the details of the DFT+DMFT calculations see in Supplementary Materials (SM).

In order to account for the thermal contribution to the lattice free energy it requires to evaluate the phonon dispersion relations of PM FeO within DFT+DMFT. This is still a challenge for the systems near the Mott IMT [52–59]. Instead, we use a more simplified Debye-Grüneisen model in which the effects of quasiharmonic contributions are taken by approximate description of the Grüneisen parameter using the Dugdale-McDonald's formula [51]. It gives a reliable estimate for the evolution of the Poisson ratio, Grüneisen ratio, and Debye temperature as a function of lattice volume. (We note however that this model does not include the effects of anharmonicity and vibrational instability which seems to be relevant, e.g., near the triple point). The local magnetic moments entropy contribution is estimated as $\Delta S_{mag} = R\ \ln(M_{loc} + 1)$ (see [60] and reference therein), where $M_{loc} \equiv \langle \hat{m}_z^2 \rangle^{1/2}$ is the instantaneous local moment of Fe ion evaluated in DMFT. Our results for the phase diagram are summarized in Fig. 1. Our results for the phase stability, equation of state and local magnetic moments obtained from the DFT+DMFT calculations for a temperature near 1200 K are shown in Fig. 2.

Our calculations indicate that FeO is a B1-structured Mott insulator at pressures below ∼40-60 GPa, with a large (∼2 eV) energy gap between the Fe $3d$ states (Fig. 3), in agreement with previous findings [15, 17, 18]. Fluctuating atomic-scale magnetic moments of ∼3.6 μ_B imply a HS $S = 2$ state for the Fe^{2+} ion, as expected for the $3d^6$ configuration in an octahedral crystal field (e.g., see Fig. 2 of Ref. [11]). Under pressure, FeO exhibits electronic transitions, followed by crystal-structural transformations. We find a Mott IMT for the B1 phase at about 70 GPa and 1500 K, in accord with past shock-wave and static measurements [4–8]. In addition, our analysis of the pressure and temperature dependence of the spectral function of FeO calculated within DFT+DMFT implies a negative Clapeyron slope for the Mott IMT, suggestive of Fermi-liquid behavior and consistent with recent experimental results [9, 13–16, 33]. As the volume change is calculated to be small (< 1%), even a small (positive) entropy change can explain the temperature-dependence of the metallization transition.

Our results show that at high temperatures the Mott IMT does not overlap with the HS-LS transition of iron. Instead, the spin and metallization transitions appear to

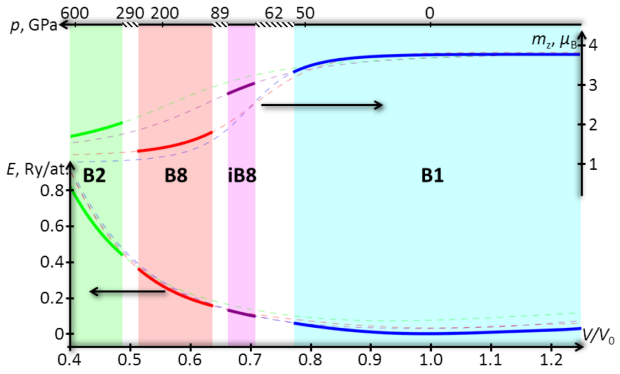

FIG. 2: Total energy (bottom) and instantaneous local magnetic moment $\sqrt{\langle \hat{m}_z^2 \rangle}$ (top) of PM FeO as a function of volume, as obtained by DFT+DMFT calculations for different phases at a temperature $T = 1160$ K. Colors indicate the stability ranges of different crystallographic phases.

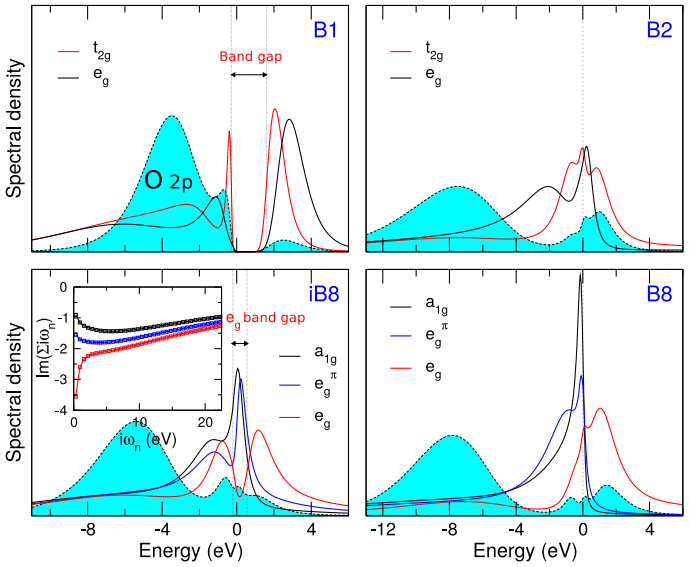

FIG. 3: Partial spectral functions showing the electron-orbital contributions to bonding in different phases of PM FeO, as calculated by DFT+DMFT at $T = 1160$ K. Contributions from Fe $3d$ states (t_{2g}, or its split a_{1g}, e_g^π components, and e_g states) are shown by solid curves, and O $2p$ states are given by shaded area (cyan). For iB8 FeO the inset shows a Matsubara plot of the imaginary part of the self-energy, $\mathrm{Im}\Sigma(i\omega_n)$.

	V_0^{HS}	$K_{0,T}^{\mathrm{HS}}$	V_0^{LS}	$K_{0,T}^{\mathrm{LS}}$	$P_{\mathrm{tr.}}^{\mathrm{HS-LS}}$	$\Delta V/V$ (%)
B1	144.1	140	122.4	210	73	9
B2	133.7	136	110.8	256	116	6
iB8	138.1	143	119.6	227	62	7
B8	143.3	128	114	274	43	13

TABLE I: Parameters of the third-order Birch-Murnaghan equation of states of PM FeO phases, as evaluated from the DFT+DMFT total energy results at an electronic temperature $T = 1160$ K. V_0 is volume and $K_{0,T}$ isothermal bulk modulus (subscript zero indicates zero pressure, $P = 0$, and $dK_{0,T}/dP$ is fixed to 4.1).

be decoupled, and our calculations reveal the existence of a novel Fe HS metallic phase over the ∼40-150 GPa pressure range at temperatures between 1500 and 4000 K, with transition to the LS state at conditions near to those of the core-mantle boundary (Fig. 1). The spin-state transition in the metallic B1 phase has a positive P-T slope. While the B1 LS phase has a considerably smaller unit-cell volume and hence larger bulk modulus, by ∼ 9% and 48%, respectively, at about 110 GPa and 2500 K, we expect a broad phase boundary at the HS-LS B1 phase transition at high pressure and temperature conditions. It is also likely that the spin transition is spread out over a finite pressure range – hence depth interval – in Earth's mantle, despite the sizable change of properties involved. The B1 structure remains stable at the high temperatures of Earth's mantle and outer core, and the high-spin metallic form of this structure is proposed to be stable near core-mantle boundary conditions (Fig. 1).

Below 1500 K, the non-metallic, HS B1 phase transforms to the inverse B8 (iB8, anti-NiAs) structure above ∼62 GPa (Fig. 2). Our results suggest that the unit-cell volume drops by ∼10.7% (while most likely this change spreads out over a broad pressure range), with only a slight increase in bulk modulus, from 140 to 143 GPa. The iB8 phase is still in a HS state (local moment ∼3 μ_B upon compression to ∼0.7 V_0), but the trigonal prismatic coordination of the iron site causes orbital-selective collapse of the local moments [61]. In fact, while the Fe a_{1g} states are metallic and show a quasiparticle peak at the Fermi level, a small energy gap remains for the Fe e_g states (see Fig. 3). It is seen as a divergence of the imaginary part of the Fe e_g self-energy $\mathrm{Im}\Sigma(\omega_n)$ at the lowest Matsubara frequencies (see the inset of Fig. 3).

The iB8 phase then transforms to the normal B8 (NiAs) structure above 89 GPa (at ∼1200 K), with a small reduction in unit-cell volume (∼2.1%) but a near doubling of the bulk modulus to 274 GPa. The transition involves a collapse of local magnetic moments into the LS state (∼0.9 μ_B, see Fig. 2), and appearance of correlated metallic behavior. The B2 (CsCl) structure, which is stable above 290 GPa at ∼1200 K, is also a LS, correlated-electron metal, as indicated by the lack of a band gap in the spectral density and the low value of local moments (Figs. 2, 3).

Our results thus suggest that wüstite, which may appear in the lowermost mantle due to chemical reactions at the core-mantle boundary, is metallic and could produce seismological anomalies caused by spin-state transitions at deep-mantle depths (∼1700-2000 km). Enhanced electrical conductivity due to the presence of metallic FeO would influence heat transfer from Earth's core into the mantle, as well as the temporal evolution of magnetic field lines crossing into the lower mantle. From the perspective of phase stability, it is notable that the metallization and spin-state transitions are *decoupled* for the

B1 phase of FeO at high temperatures (Fig. 1).

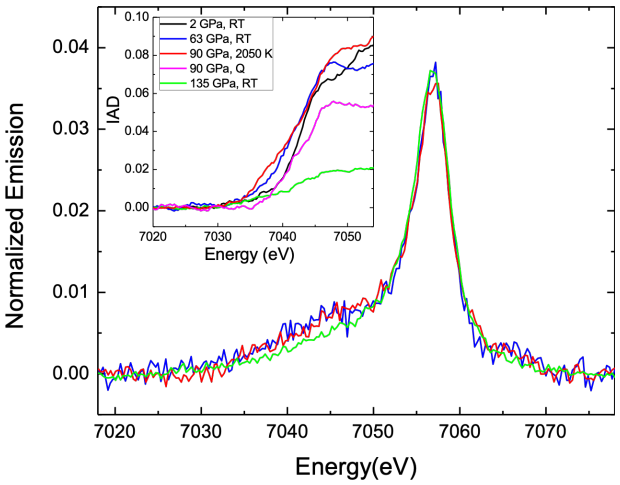

FIG. 4: Fe K_β x-ray emission spectra collected from FeO at high pressure as a function of temperature. The spectra have been normalized and shifted so that the main peak is centered around 7058 eV. Inset: Integrated absolute difference (IAD) for a few of the collected spectra. The abundance of the HS state remains close to 100% up to 74 GPa, and decreases appreciably upon further compression [90 GPa quenched (Q) and 135 GPa room temperature (RT)]. We observe complete recovery (with 100% abundance) of the HS state, and completion of the rB1-B1 structural transition, upon heating to 2050 K (spectrum at 90 GPa, 2050 K).

To verify these results, and specifically to confirm the existence of the HS Fe in the metallic B1 phase, we used XES and XRD to characterize FeO at 60-140 GPa and temperatures up to 2100 K (Fig. 4). Such a combined experimental study is technically challenging, and has rarely been attempted [42, 62]. Our x-ray spectroscopy was conducted on samples with stoichiometry $Fe_{0.94}O$ (see SM for the details) at beamline 13-IDD of the Advanced Photon Source, Argonne National Laboratory. For combined XRD and XES measurements at high pressures and temperatures, a XES system was added to the 13-IDD beamline that includes laser heating for XRD with diamond-anvil cells. Our diffraction measurements were performed at a wavelength of $\lambda = 0.4959$ Å with a Mar165 CCD detector. Iron $K_{\beta 1,3}$ spectra were collected using an excitation energy of 10.75 keV with a spot size of $\sim 4 \times 4$ μm, and a curved Si 440 analyzer ($a = 5.431$ Å) in a Rowland circle spectrometer geometry having nominal spherical diameter of ∼1000 mm (an Fe wire is used to calibrate the analyzer angle of 66.18°, assuming that the main peak is at 7058 eV). Spectra were collected from 7018 to 7078 eV in ∼0.3 eV steps (1-10 s collection time for each step), with each measurement repeated an even number of times (2-10). At each step the entire region-of-interest on the detector is summed, and the final spectrum is a summation of all repetitions. A sample of siderite $FeCO_3$ at 60 GPa was used as a low-spin standard [63] in order to evaluate the integrated absolute difference (IAD) between the sample and the LS $FeCO_3$ as IAD $= \int_{E_i}^{E_f} |I_{norm}^{\text{shifted}}(E) - I_{norm}^{\text{FeCO}_3}(E)|dE$, where $I_{norm}(E)$ is the normalized to a unit background-subtracted spectrum $I_{norm}(E) = I(E)/\int_{7018}^{7065} |I(E)|dE$; $E_i \sim 7030$ eV is just before the satellite peak, $E_f \sim 7045$ eV, above (see SM).

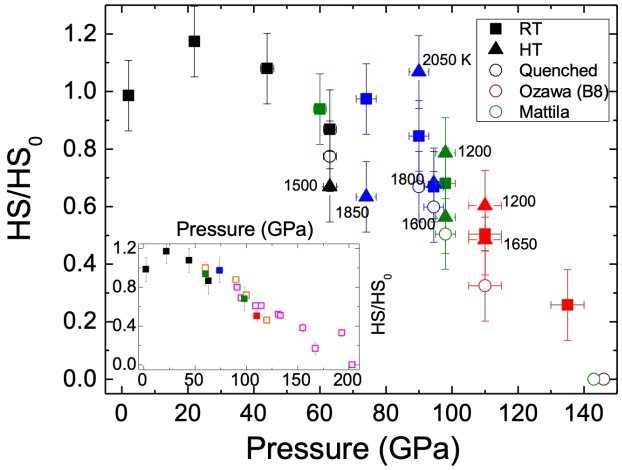

FIG. 5: A relative abundance of the Fe HS state to that at ambient pressure (HS_0) at high pressures and either room temperature (RT) or high temperature (HT), as calculated from IAD obtained from XES (squares, triangles and circles represent RT, HT and quenched data, respectively). Colors represent data collected from different sample runs. Note that Ozawa *et al.* and Mattila *et al.'s* data were obtained after laser-heating, resulting in a structural transition into the B8 phase [33, 64]. Inset: HS/HS_0 abundance at RT (unheated samples), revealing the sluggish spin transition induced by pressure alone. Open magenta and orange squares represent the RT Mössbauer spectroscopy results obtained by Hamada *et al.* [65] and Pasternak *et al.* [20].

At room temperature, we find the iron to be in the HS state up to 74 GPa, with the LS Fe appearing on further compression: the ratio of high- to low-spin iron in FeO drops to about 50% by 110 GPa (Fig. 5). This is in agreement with Mössbauer measurements [20] and recent DFT+DMFT calculations [15, 17–19], but is not entirely consistent with prior XES work [21]. We attribute this difference to the previous x-ray spectroscopy having probed the sample from the side (through a Be gasket), across the sample's full pressure distribution, making it difficult to see the disappearance of the K_β shoulder that is the signature of the LS state. We note that FeO is in the distorted (rB1) form of the B1 structure over most of this pressure range [4, 13, 14], with the sluggish spin transition starting in the rB1 phase and being followed by transformation to the B8 phase at room temperature. Therefore, consistent with our DFT+DMFT calculations we conclude that the electronic-spin and structural transitions are decoupled.

With increasing temperature near 90 GPa, XRD shows the presence of the low-temperature rB1 structure up to about 1800 K, and completion of the rB1-to-B1 phase transition – with the iron 100% in the HS state –

upon heating to 2050 K (Fig. 1). Our experiments do not confirm the previously reported LS B1 phase of FeO above ∼70 GPa at temperatures above 1300 K [14, 15, 17, 34], but they are in qualitative agreement with our DFT+DMFT calculations. Furthermore, we note the sensitivity of the spin state to changes in the crystal-field splitting of the Fe 3*d* energy levels across the rB1-B1 phase transformation of FeO.

We thus conclude from both experiment and theory that a novel HS B1-type phase of FeO appears near conditions relevant to Earth's core-mantle boundary. Therefore, if present in this region, as might be expected due to chemical reactions between mantle rock and liquid metal of the core, FeO can contribute to the seismological anomalies of the D" region, and cause lateral variations in heat flow into the base of the mantle (e.g., Ref. [12]).

Our DFT+DMFT results are for crystalline phases, so it is premature to make quantitative predictions about the properties of Earth's fluid outer core [66]. Nevertheless, the evidence we have found for significant changes in bulk sound velocity ($\sqrt{K}/\rho$) across both structural (B8-B2: about -5%) and electronic (HS-LS: about +10%) transitions in metallic FeO raises the possibility of anomalous variations in seismic-wave velocity with depth through the core. Specifically, it may be imprudent to treat the outer core as though it followed the isentropic equation of state of a single phase, because changes in liquid and electronic structures could cause subtle variations in the depth dependence of seismic-wave velocity throughout this region. Our results also prompt further investigation of the electronic states of Earth's lower-mantle minerals as possible sources of seismic and chemical heterogeneity, as well as thermal instabilities.

Acknowledgments

The authors would like to thank H. Yang, J.F. Lin and J. Liu for their assistance in preparations for the experiment, C. Kenney-Benson for assistance with handling Be, and P. Chow for assistance in preparing the XES setup at the beamline. Portions of this work were performed at GeoSoilEnviroCARS (The University of Chicago, Sector 13), Advanced Photon Source (APS), Argonne National Laboratory. GeoSoilEnviroCARS is supported by the National Science Foundation-Earth Sciences (EAR-1634415) and Department of Energy-GeoSciences (DE-FG02-94ER14466). This research used resources of the Advanced Photon Source, a U.S. Department of Energy (DOE) Office of Science User Facility operated for the DOE Office of Science by Argonne National Laboratory under Contract No. DE-AC02-06CH11357. A portion of this work was performed at HPCAT (Sector 16), Advanced Photon Source (APS), Argonne National Laboratory. HPCAT operations are supported by DOE-NNSA under Award No. DE-NA0001974, with partial instrumentation funding by NSF. The Advanced Photon Source is a U.S. Department of Energy (DOE) Office of Science User Facility operated for the DOE Office of Science by Argonne National Laboratory under Contract No. DE-AC02-06CH11357. Computing support for this work (R.N., A.L., and R.Q.H.) came from the LLNL Computing Grand Challenge program. This work performed under the auspices of the U.S. DOE by LLNL under Contract DE-AC52-07NA27344. R.J. acknowledges support from the U.S. Department of Energy and University of California. This research was supported in part by Israeli Science Foundation Grant #1189/14, #1552/18, and #1748/20. I.V.L. acknowledges support by the state assignment of Minobrnauki of Russia (Theme "Electron" No. 122021000039-4). Theoretical analysis of structural properties was supported by Russian Science Foundation (project No. 19-72-30043).

[1] Ringwood, A. E. Composition of the core and implications for the origin of the Earth. *Geochem. J.* **11**, 111 (1977).

[2] Rubie, D. C., Gessmann, C. K., Frost, D. J. Partitioning of oxygen during core formation on the Earth and Mars. *Nature* **429**, 58 (2004).

[3] Anderson, D. L. Theory of the Earth. (Blackwell, Boston, 1989).

[4] Yagi, T., Suzuki T., Akimoto, S. Static compression of wüstite ($Fe_{0.98}O$) to 120 GPa. *J. Geophys. Res.* **90**, 8784 (1985).

[5] Knittle, E., Jeanloz, R. The high-pressure phase diagram of $Fe_{0.94}O$: a possible constituent of the Earth's core. *J. Geophys. Res.* **96**, 16169 (1991).

[6] Fei, Y., Mao, H. In situ determination of the NiAs phase of FeO at high pressure and temperature. *Science* **266**, 1678 (1994).

[7] Fei, Y. Crystal chemistry of FeO at high pressure and temperature, in: Dyar, M. D., McCammon, C., Shaefer, M. W. (Eds.), Mineral spectroscopy: a tribute to Roger Burns. (Geochemical Society, Houston, 1996), pp. 243-254.

[8] Mao, H.-K., Shu, J., Fei, F., Hu, J., Hemley, R. J. The wüstite enigma. *Phys. Earth. Planet. Inter.* **96**, 135 (1996).

[9] Ozawa, H., Takahashi, F., Hirose, K., Ohishi, Y, Hirao, N. Phase Transition of FeO and Stratification in Earth's Outer Core. *Science* **334**, 792 (2011).

[10] Coppari, F., Smith, R. F., Wang, J., Millot, M., Kim, D., Rygg, J. R., Hamel, S., Eggert, J. H., Duffy, T. S. Implications of the iron oxide phase transition on the interiors of rocky exoplanets. *Nat. Geosci.* **14**, 121 (2021).

[11] Lin, J.-F., Speziale, S., Mao, Z., Marquart, H. Effects of the electronic spin transitions of iron in lower mantle

minerals: Implications for deep mantle geophysics and geochemistry. *Rev. Geophys.* **51**, 244 (2013).
[12] Manga, M., Jeanloz, R. Implications of a metal-bearing chemical boundary layer in D" for mantle dynamics. *Geophys. Res. Lett.* **23**, 3091 (1996).
[13] Fischer, R. A., *et al.* Equation of state and phase diagram of FeO. *Earth Planet. Sci. Lett.* **304**, 496 (2011).
[14] Fischer, R. A., *et al.* Phase transition and metallization of FeO at high pressures and temperatures. *Geophys. Res. Lett.* **38**, L24301 (2011).
[15] Ohta, K., *et al.* Experimental and Theoretical Evidence for Pressure-Induced Metallization in FeO with Rocksalt-Type Structure. *Phys. Rev. Lett.* **108**, 026403 (2012).
[16] Murakami, M., *et al.* High pressure and high temperature phase transitions of FeO. *Phys. Earth Planet. Int.* **146**, 273 (2004).
[17] Leonov, I. Metal-insulator transition and local-moment collapse in FeO under pressure. *Phys. Rev. B* **92**, 085142 (2015).
[18] Leonov, I., Pourovskii, L., Georges, A., Abrikosov, I.A. Magnetic collapse and the behavior of transition metal oxides at high pressure. *Phys. Rev. B* **94**, 155135 (2016).
[19] Leonov, I., Shorikov, A. O., Anisimov, V. I., Abrikosov, I. A. Emergence of quantum critical charge and spin-state fluctuations near the pressure-induced Mott transition in MnO, FeO, CoO, and NiO. *Phys. Rev. B* **101**, 245144 (2020).
[20] Pasternak, M. P., Taylor, R. D., Jeanloz, R. Li, X., Nguyen, J. H., McCammon, C. A. High Pressure Collapse of Magnetism in $Fe_{0.94}O$: Mössbauer Spectroscopy Beyond 100 GPa. *Phys. Rev. Lett.* **79**, 5046 (1997).
[21] Badro, J., *et al.* Magnetism in FeO at megabar pressures from x-Ray emission spectroscopy. *Phys. Rev. Lett.* **83**, 4101 (1999).
[22] Fischer, R. A., Campbell, A. J. High pressure melting of wüstite. *Am. Mineral.* **95**, 1473 (2010).
[23] Wu, Z., Justo, J. F., da Silva, C. R. S., de Gironcoli, S., Wentzcovitch, R. M. Anomalous thermodynamic properties in ferropericlase throughout its spin crossover. *Phys. Rev. B* **80**, 014409 (2009).
[24] Wu, Z., Justo, J. F., Wentzcovitch, R. M. Elastic Anomalies in a Spin-Crossover System: Ferropericlase at Lower Mantle Conditions *Phys. Rev. Lett.* **110**, 228501 (2013).
[25] Hsu, H., Wentzcovitch, R. M. First-principles study of intermediate-spin ferrous iron in the Earth's lower mantle *Phys. Rev. B* **90**, 195205 (2014).
[26] Lavina, B., *et al.* Discovery of the recoverable high-pressure iron oxide Fe_4O_5. *Proc. Natl Acad. Sci. USA* **108**, 17281 (2011).
[27] Layek, S., *et al.* Verwey-Type Charge Ordering and Site-Selective Mott Transition in Fe_4O_5 under Pressure. *J. Am. Chem. Soc.* **144**, 10259 (2022).
[28] Hu, Q., Kim, D. Y., Yang, W., Yang, L., Meng, Y., Zhang, L., Mao, H. K. FeO_2 and FeOOH under deep lower-mantle conditions and Earth's oxygen-hydrogen cycles. *Nature (London)* **534**, 241 (2016).
[29] Koemets, E., *et al.* Revealing the Complex Nature of Bonding in the Binary High-Pressure Compound FeO_2. *Phys. Rev. Lett.* **126**, 106001 (2021).
[30] Bykova, E., *et al.* Structural Complexity of Simple Fe_2O_3 at High Pressures and Temperatures. *Nat. Commun.* **7**, 10661 (2016).
[31] Greenberg, E., *et al.* Pressure-Induced Site-Selective Mott Insulator-Metal Transition in Fe_2O_3. *Phys. Rev. X* **8**, 031059 (2018).
[32] Wan, T., Sun, Y., Wentzcovitch, R. M. Intermediate spin state and the B1-B2 transition in ferropericlase *Phys. Rev. Research* **4**, 023078 (2022).
[33] Ozawa, H., *et al.* Spin crossover, structural change, and metallization in NiAs-type FeO at high pressure. *Phys. Rev. B* **84**, 134417 (2011).
[34] Cohen, R. E., Mazin I. I., Isaak, D. G. Magnetic Collapse in Transition Metal Oxides at High Pressure: Implications for the Earth. *Science* **275**, 654 (1997).
[35] Sun, Y., Cococcioni, M., Wentzcovitch, R. M. LDA+U_{sc} calculations of phase relations in FeO. *Phys. Rev. Materials* **4**, 063605 (2020).
[36] Ozawa, H., Hirose, K., Tateno, S., Sata, N., Ohishi, Y., Phase transition boundary between B1 and B8 structures of FeO up to 210 GPa. *Phys. Earth Planet. Inter.* **179**, 157 (2010).
[37] Kondo, T., Ohtani, E., Hirao, N., Yagi, T., Kikegawa, T., Phase transitions of (Mg,Fe)O at megabar pressures. *Phys. Earth Planet. Inter.* **143**–**144**, 201 (2004).
[38] Georges, A., Kotliar, G., Krauth, W., Rezonberg, M. J. Dynamical mean-field theory of strongly correlated fermion systems and the limit of infinite dimensions. *Rev. Mod. Phys.* **68**, 13 (1996).
[39] Kotliar, G., *et al.* Electronic structure calculations with dynamical mean-field theory. *Rev. Mod. Phys.* **78**, 865 (2006).
[40] Haule, K., Quantum Monte Carlo impurity solver for cluster dynamical mean-field theory and electronic structure calculations with adjustable cluster base. *Phys. Rev. B* **75**, 155113 (2007).
[41] Pourovskii, L. V., Amadon, B., Biermann, S., Georges, A. Self-consistency over the charge density in dynamical mean-field theory: A linear muffin-tin implementation and some physical implications. *Phys. Rev. B* **76**, 235101 (2007).
[42] Lin, J.-F., *et al.* X-ray emission spectroscopy with a laser-heated diamond anvil cell: a new experimental probe of the spin state of iron in the Earth's interior. *J. Synchrotron Radiat.* **12**, 637 (2005).
[43] Baroni, S., de Gironcoli, S., Dal Corso, A., Giannozzi, P. Phonons and related crystal properties from density-functional perturbation theory. *Rev. Mod. Phys.* **73**, 515 (2001).
[44] Giannozzi, P., *et al.* QUANTUM ESPRESSO: a modular and open-source software project for quantum simulations of materials. *J. Phys.: Condens. Matter* **21**, 395502 (2009).
[45] Gull, E., Millis, A. J., Lichtenstein, A. I., Rubtsov, A. N., Troyer, M., Werner, P. Continuous-time Monte Carlo methods for quantum impurity models. *Rev. Mod. Phys.* **83**, 349 (2011).
[46] Marzari, N., Mostofi, A. A., Yates, J. R. Souza, I., Vanderbilt, D. Maximally localized Wannier functions: Theory and applications. *Rev. Mod. Phys.* **84**, 1419 (2012).
[47] Anisimov, V. I., *et al.* Full orbital calculation scheme for materials with strongly correlated electrons. *Phys. Rev. B* **71**, 125119 (2005).
[48] Korotin, D., *et al.* Construction and solution of a Wannier-functions based Hamiltonian in the pseudopotential plane-wave framework for strongly correlated materials. *Eur. Phys. J. B* **65**, 91 (2008).
[49] Anisimov, V. I., Gunnarsson, O. Density-functional calculation of effective Coulomb interactions in metals.

Phys. Rev. B **43**, 7570 (1991).

[50] Timrov, I., Marzari, N., Cococcioni, M. Self-consistent Hubbard parameters from density-functional perturbation theory in the ultrasoft and projector-augmented wave formulations *Phys. Rev. B* **103**, 045141 (2021).

[51] Moruzzi, V. L., Janak J. F., Schwarz, K. Calculated thermal properties of metals. *Phys. Rev. B* **37**, 790 (1988).

[52] Dai, X., Savrasov, S. Y., Kotliar, G., Migliori, A., Ledbetter, H., Abrahams, E. Calculated Phonon Spectra of Plutonium at High Temperatures. *Science* **300**, 953 (2003).

[53] Floris, A., de Gironcoli, S., Gross, E. K. U., Cococcioni, M. Vibrational properties of MnO and NiO from DFT+U-based density functional perturbation theory. *Phys. Rev. B* **84**, 161102(R) (2011).

[54] Leonov, I., Poteryaev, A. I., Anisimov, V. I., Vollhardt, D. Calculated phonon spectra of paramagnetic iron at the α-γ phase transition. *Phys. Rev. B* **85**, 020401(R) (2012).

[55] Leonov, I., Poteryaev, A. I., Gornostyrev, Yu. N., Lichtenstein, A. I., Katsnelson, M. I., Anisimov, V. I., Vollhardt, D. Electronic correlations determine the phase stability of iron up to the melting temperature. *Sci. Rep.* **4**, 5585 (2014).

[56] Han, Q., Birol, T., Haule, K. Phonon Softening due to Melting of the Ferromagnetic Order in Elemental Iron. *Phys. Rev. Lett.* **120**, 187203 (2018).

[57] Koçer, C. P., Haule, K., Pascut G. L., Monserrat, B. Efficient lattice dynamics calculations for correlated materials with DFT+DMFT. *Phys. Rev. B* **102**, 245104 (2020).

[58] Marcondes, M. L., Zheng, F., Wentzcovitch, R. W. Phonon dispersion throughout the iron spin crossover in ferropericlase. *Phys. Rev. B* **102**, 104112 (2020).

[59] Nakano, K., Morresi, T., Casula, M., Maezono, R., Sorella, S. Atomic forces by quantum Monte Carlo: Application to phonon dispersion calculations. *Phys. Rev. B* **103**, L121110 (2021).

[60] Chuang, Y.-Y., Schmid, R., Chang Y.-A. Magnetic contributions to the thermodynamic functions of pure Ni, Co, and Fe. *Metallurg. Trans. A* **16A**, 153 (1985).

[61] de'Medici, L., Georges, A., Biermann, S. Orbital-selective Mott transition in multiband systems: Slave-spin representation and dynamical mean-field theory. *Phys. Rev. B* **72**, 205124 (2005).

[62] Lin, J.-F., *et al.* Spin Transition Zone in Earth's Lower Mantle, *Science* **317**, 1740 (2007).

[63] Mattila, A., Pylkkäen, T., Rueff, J.-P., Huotari, S., Vankó, G., Hanfland, M., Lehtinen, M., Hämäläinen, K. Pressure induced magnetic transition in siderite $FeCO_3$ studied by x-ray emission spectroscopy, J. Phys.: Condens. Matter **19**, 386206 (2007).

[64] Mattila, A., Rueff, J.-P., Badro, J., Vankó, G., Shukla, A., Metal-Ligand Interplay in Strongly Correlated Oxides: A Parametrized Phase Diagram for Pressure-Induced Spin Transitions, *Phys. Rev. Lett.* **98**, 196404 (2007).

[65] Hamada, M., *et al.* Magnetic and spin transitions in wüstite: A synchrotron Mössbauer spectroscopic study, *Phys. Rev. B* **93**, 155165 (2016).

[66] Morard, G., *et al.* Structural and Electronic Transitions in Liquid FeO Under High Pressure, *J. Geophys. Res. Solid Earth* **127**, e2022JB025117 (2022).